phys. stat. sol. (b) **242**, No. 13, 2720–2728 (2005) / **DOI** 10.1002/pssb.200541128

Quasiparticle and excitonic effects in the optical spectra of diamond, SiC, Si, GaP, GaAs, InP, and AlN

P. H. Hahn, K. Seino*, W. G. Schmidt, J. Furthmüller, and **F. Bechstedt**

Institut für Festkörpertheorie und -optik, Friedrich-Schiller-Universität, Max-Wien-Platz 1, 07743 Jena, Germany

Received 17 June 2005, revised 22 August 2005, accepted 22 August 2005
Published online 7 October 2005

PACS 71.20.Mq, 71.20.Nr, 71.35.Cc, 78.20.Bh, 78.40.Fy

We demonstrate the potential of recently developed electronic-structure methods for the calculation of the optical properties of solids. As prototypical examples semiconductors crystallizing in diamond or zinc-blende structure are studied. The many-body effects are fully taken into account by a solution of the combined Dyson and Bethe-Salpeter equations. We show that an initial-value formulation of the polarization function allows for an efficient numerical calculation of the optical susceptibility. The effect of the renormalization of electrons and holes to quasiparticles is shown for both the band structure and the optical spectrum. In addition, excitonic effects are identified to remarkably influence the optical absorption.

© 2005 WILEY-VCH Verlag GmbH & Co. KGaA, Weinheim

1 Introduction

Recent years have seen impressive methodological progress in the accurate numerical modelling of optical properties from *first principles* using the many-body perturbation theory (MBPT) [1]. It has become possible to compute single-particle electronic excitations in an accurate manner using Hedin's GW approximation (GWA) [2]. In addition, the Bethe-Salpeter equation (BSE) for electron–hole pair excitations can be solved in the framework of the same approximation, in order to account for excitonic and local-field (LF) contributions to the polarization function [3–5]. However, the large numerical effort required to solve the BSE has restricted such calculations to the interaction of relatively few electron-hole pairs. Therefore, the calculations of optical properties are usually limited to bulk semiconductors [6–10] or to semiconductor surfaces with strongly localized and energetically well separated states [11, 12]. There are only first trials to include more pair states in the calculations of optical spectra, for instance to describe surface-modified bulk excitons [13, 14]. The formalism, however, also works for strongly localized electron–hole pair excitations in highly polarizable solids and molecules [15].

In this paper the progress in the calculation of optical properties is discussed with a focus on bulk semiconductors. This does not only concerns the computation of the geometries and electronic structures but also the inclusion of many-body effects in the framework of the MBPT. We show that optical spectra such as the optical absorption can now be calculated from *first principles*. One important intermediate step is related to the quasiparticle band structures. Semiconductors crystallizing in diamond or zinc-blende structure are used as examples. In Section 2 the computational methods are described. We present a novel numerically efficient approach to solve the BSE for the polarization function in the time domain using an initial-value formulation. The quasiparticle band structures and optical absorption spectra resulting for C, SiC, Si, GaP, GaAs, InP, and AlN are discussed in detail in Section 3. A brief summary concludes the paper in Section 4.

* Corresponding author: e-mail: seino@ifto.physik.uni-jena.de, Phone: +49 3641 947168, Fax: +49 3641 947152

© 2005 WILEY-VCH Verlag GmbH & Co. KGaA, Weinheim

2 Computational methods

2.1 Modeling of ground state

In order to calculate the surface optical spectra we proceed in three steps. First, the energetically favored geometry is determined. The required total-energy and electronic-structure calculations are based on the density functional theory (DFT) [16] and the local density approximation (LDA) [17]. We are using two different implementations of the underlying DFT-LDA. In the case of crystalline Si we have checked that the two methods practically give the same results. In the first version the electron-ion interaction is described by nonlocal norm-conserving pseudopotentials [18]. Semicore states are taken into account by nonlinear core corrections to the exchange and correlation energy. A massively parallel, real-space finite-difference method [19] is used to deal with the large unit cells. A multigrid technique accelerates the convergence. The spacing of the finest grid used to represent the electronic wave functions and charge density is about 10% of a bulk bond length. The second implementation is based on the Vienna Ab-initio Simulation Package (VASP) [21]. The pseudopotentials are generated according to the projector-augmented wave (PAW) method to describe the interaction between atomic cores and valence electrons [22]. The all-electron PAW wave functions of these electrons determine the optical matrix elements [23]. In the case of the PAW pseudopotentials the energy cutoffs of the plane-wave expansions of the Bloch states to obtain converged results are relatively low. Indeed, Fig. 1 shows that optical response calculations based on the two different implementations of the DFT-LDA give almost the same spectrum.

2.2 Frequency-dependent dielectric function

We take advantage of the translational symmetry. The Bloch picture is valid with wave vectors $\boldsymbol{k}$ from the surface Brillouin zone (BZ) and band indizes ν as good quantum numbers. Within the LDA to exchange and correlation the single-particle Kohn–Sham (KS) equation yields eigenfunctions $|\nu\boldsymbol{k}\rangle$ (or $\psi_{\nu\boldsymbol{k}}(\boldsymbol{x}) = \langle \boldsymbol{x}|\nu\boldsymbol{k}\rangle$) and eigenvalues $\varepsilon_\nu(\boldsymbol{k})$. The macroscopic dielectric function is related to the polarization function P. Within the Bloch picture one has for a cubic system [5, 20]

$$\varepsilon(\omega) = 1 - \frac{8\pi e^2\hbar^2}{V} \sum_{c,v,\boldsymbol{k}} \sum_{c',v',\boldsymbol{k}'} \{M^j_{cv}(\boldsymbol{k})\, M^{j*}_{c'v'}(\boldsymbol{k}')\, P(cv\boldsymbol{k}, c'v'\boldsymbol{k}'; \omega) + c.c. \quad \text{and} \quad \omega \leftrightarrow -\omega\} \tag{1}$$

with matrix elements of the velocity operator $\boldsymbol{v}$

$$M^j_{cv}(\boldsymbol{k}) = \frac{\langle c\boldsymbol{k}|\, v_j |v\boldsymbol{k}\rangle}{\varepsilon_c(\boldsymbol{k}) - \varepsilon_v(\boldsymbol{k})} \tag{2}$$

and V as the normalization volume. In (1) the sums run over pairs of electrons in empty conduction band states $|c\boldsymbol{k}\rangle$ and holes in occupied valence band states $|v\boldsymbol{k}\rangle$, which are virtually or physically excited by photons. The effect of the photon wave vector is neglected.

The polarization function P obeys a BSE. Neglecting the coupling of resonant and antiresonant electron–hole pairs as well as the non-particle-conserving contributions to the electron–hole interaction, the BSE obeys the form

$$\sum_{c'',v'',\boldsymbol{k}''} \{H(cv\boldsymbol{k}, c''v''\boldsymbol{k}'') - \hbar(\omega + i\gamma)\, \delta_{cc''}\delta_{vv''}\delta''_{\boldsymbol{kk}}\}\, P(c''v''\boldsymbol{k}'', c'v'\boldsymbol{k}'; \omega) = -\delta_{cc'}\delta_{vv'}\delta'_{\boldsymbol{kk}} \tag{3}$$

with the effective electron–hole pair Hamiltonian $H(cv\boldsymbol{k}, c'v'\boldsymbol{k}')$ and a small damping γ of the pair excitations. The Hamiltonian of pairs of excited electrons and holes, more precisely, of quasielectrons and quasiholes, is given by [3, 6, 20]

$$H(cv\boldsymbol{k}, c'v'\boldsymbol{k}') = \left[\varepsilon^{QP}_c(\boldsymbol{k}) - \varepsilon^{QP}_v(\boldsymbol{k})\right] \delta_{cc'}\delta_{vv'}\delta'_{\boldsymbol{kk}} + W(cv\boldsymbol{k}, c'v'\boldsymbol{k}') + \overline{v}(cv\boldsymbol{k}, c'v'\boldsymbol{k}') \tag{4}$$

© 2005 WILEY-VCH Verlag GmbH & Co. KGaA, Weinheim

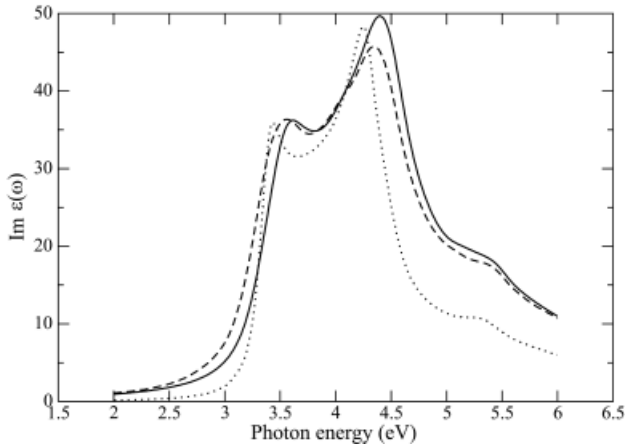

Fig. 1 Comparison of the imaginary part of the dielectric function for Si computed with wave functions from the real-space implementation of the DFT-LDA (solid line) and from the PAW approach (dashed line) and 1000 random $\boldsymbol{k}$-points. The many-body effects have been taken into account (see below). The spectra are compared with an experimental curve (dotted line) [24].

with the matrix elements

$$W(cv\boldsymbol{k}, c'v'\boldsymbol{k}') = -\int d^3\boldsymbol{x} \int d^3\boldsymbol{x}' \psi^*_{c\boldsymbol{k}}(\boldsymbol{x})\, \psi_{c'\boldsymbol{k}'}(\boldsymbol{x})\, W(\boldsymbol{x}, \boldsymbol{x}')\, \psi_{v\boldsymbol{k}}(\boldsymbol{x}')\, \psi^*_{v'\boldsymbol{k}'}(\boldsymbol{x}') \tag{5}$$

and

$$\bar{v}(cv\boldsymbol{k}, c'v'\boldsymbol{k}') = 2 \int d^3\boldsymbol{x} \int d^3\boldsymbol{x}' \psi^*_{c\boldsymbol{k}}(\boldsymbol{x})\, \psi_{v\boldsymbol{k}}(\boldsymbol{x})\, \bar{v}(\boldsymbol{x} - \boldsymbol{x}')\, \psi_{c'\boldsymbol{k}'}(\boldsymbol{x}')\, \psi^*_{v'\boldsymbol{k}'}(\boldsymbol{x}') \tag{6}$$

of the (statically) screened Coulomb interaction $W(\boldsymbol{x}, \boldsymbol{x}')$ [25] and a bare Coulomb interaction $\bar{v}(\boldsymbol{x} - \boldsymbol{x}')$. Only the short-range part of the latter is taken into account in agreement with the physical character of expression (6) as electron–hole exchange [4].

The screened contribution W (5) to the total electron–hole interaction includes the classical attraction of electron and hole as represented by the diagonal elements $c = c'$ and $v = v'$. It is responsible for the electron–hole binding in the Wannier–Mott limit [26]. The other contributions represent the mixing of electron–hole pairs which is responsible for the redistribution of oscillator strength in optical spectra [6, 7, 20]. The electron–hole exchange term $\propto \bar{v}$ (7) [3, 27, 28] corresponds to the inclusion of LF effects [29, 30]. Indeed, in the bulk case it has been shown [28, 31] that the inclusion of $\bar{v}$ in the BSE (3) gives a polarization corresponding to the macroscopic dielectric susceptibility.

The excited electrons and holes also interact as individual particles with the inhomogeneous electron gas of the system. This leads to an exchange-correlation self-energy Σ of the system beyond the exchange-correlation potential V_{XC} that is already used in the Kohn–Sham equation of the DFT-LDA. As a consequence, this renormalization gives rise to quasielectrons and quasiholes [1, 2]. Assuming the same energetical ordering of the positions of the quasiparticle peaks and of the KS energies, the quasiparticle effects are included within first-order perturbation theory [32, 33]. The KS wave functions are not updated [34] and the DFT-LDA eigenvalues are corrected according to

$$\varepsilon^{QP}_{v}(\boldsymbol{k}) = \varepsilon_{v}(\boldsymbol{k}) + \Delta_{v}(\boldsymbol{k}), \tag{7}$$

$$\Delta_{v}(\boldsymbol{k}) = \langle v\boldsymbol{k}|\, \Sigma\left(\varepsilon^{QP}_{v}(\boldsymbol{k})\right) - V_{XC}|\, v\boldsymbol{k}\rangle. \tag{8}$$

The exchange-correlation self-energy operator Σ is taken within the GWA [2]. In the explicit calculations we introduce further approximations following the schemes by Hybertsen and Louie [35] and Bechstedt et al. [36] or Cappellini et al. [37]. For several semiconductors and their surfaces this approximate treatment of the self-energy corrections (8) has been shown to result in excitation energies which are within 0.1 eV of the experimental values [13, 38].

The rank of the Hamiltonian matrix (4) is determined by the number of electron–hole pair slabs $|cv\boldsymbol{k}\rangle$ contributing to the optical spectrum. The number of pairs of conduction bands c and valence bands v

© 2005 WILEY-VCH Verlag GmbH & Co. KGaA, Weinheim

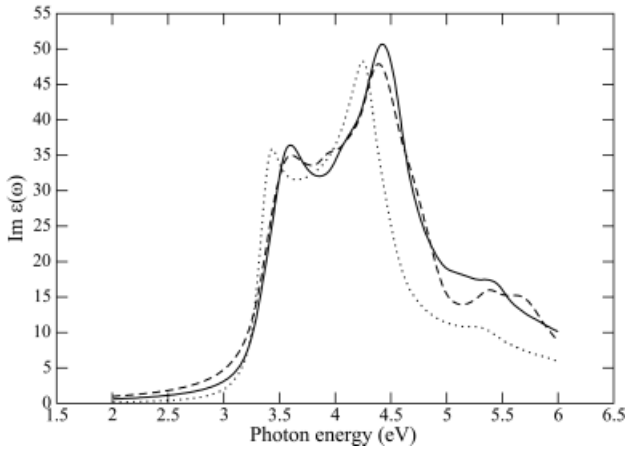

Fig. 2 Imaginary part of the dielectric function for Si computed within the real-space implementation of the DFT-LDA using 1000 randomly distributed $\boldsymbol{k}$-points (solid line) or 1000 homogeneously distributed MP $\boldsymbol{k}$-points (dashed line) in the BZ of a sc structure containing 8 Si atoms. The spectra are compared with an experimental curve (dotted line) [24].

depends on the region of photon energies $\hbar\omega$ that should be described. The $\boldsymbol{k}$-sampling of these bands in the Brillouin zone (BZ) determines the accurate computation of two effects, (i) the interband density of states weighted by the transition matrix elements (2) and (ii) the coupling of electron–hole pairs $cv\boldsymbol{k}$ and $c'v'\boldsymbol{k}'$ in different regions of the BZ. Considering the diamond and zinc-blende semiconductors in conventional unit cells with 8 atoms of the sc lattice, we found reasonable convergence for a homogeneous distribution of about 1000 $\boldsymbol{k}$-points according to Monkhorst and Pack (MP) [39] over the entire BZ with a cubic shape. We have also tested random distributions of 1000 $\boldsymbol{k}$-points over the BZ. The corresponding spectra resulting for Si are shown in Fig. 2. Our experience with many crystals is that convergence with respect to the excitonic effects mediated by the interactions (5) and (6) is faster for random $\boldsymbol{k}$-points. However, if there are pronounced density-of-state effects due to strong contributions from critical points and high-symmetry lines in the BZ, then the MP $\boldsymbol{k}$-points are better for fast convergence. The discrepancies in Fig. 2 indicate that convergence with respect to the $\boldsymbol{k}$-point sampling is most critical for the numerical treatment of excitonic effects in optical spectra. An extreme example in this respect is InN [40]. The discrepancies indicate inaccuracies of less than 0.1 eV in the determination of peak positions and of several % in the determination of peak intensities. In any case a converged $\boldsymbol{k}$-point sampling is most important to obtain the correct lineshape including the correct peak positions [41].

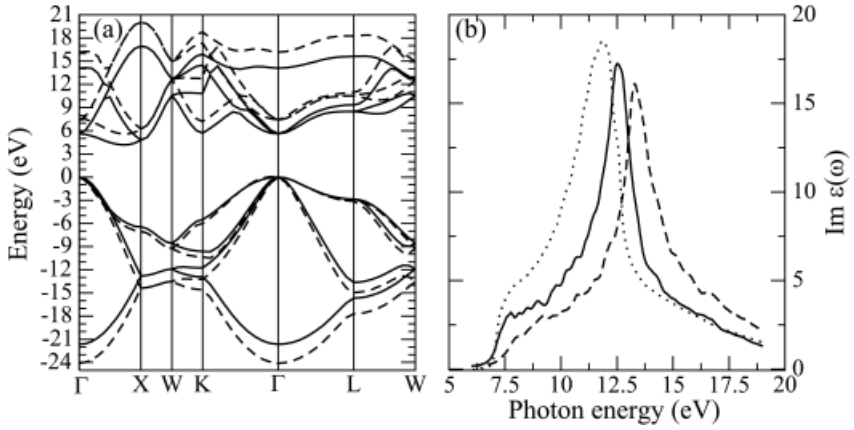

Fig. 3 Diamond: (a) Kohn–Sham (solid lines) and quasiparticle (dashed lines) band structures. Only the valence and the lowest conduction bands are shown. (b) Imaginary part of the frequency-dependent dielectric function within the independent-quasiparticle approach (dashed line), for Coulomb-correlated electron–hole pairs (solid line), and from experiment (dotted line) [44].

© 2005 WILEY-VCH Verlag GmbH & Co. KGaA, Weinheim

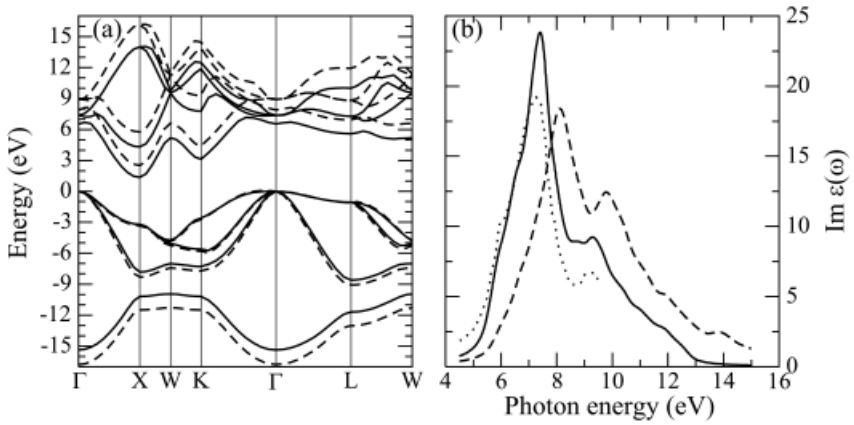

Fig. 4 Cubic SiC: Experiment from [45].

2.3 Time-dependent formulation

Since the atomic geometry of a crystal is known from the total-energy minimization procedure (cf. Section 2.1), the optical properties of a cubic semiconductor (1) can be calculated by solving the BSE (3) starting in the first step with a pair Hamiltonian (4) in DFT-LDA quality, $H(cv\boldsymbol{k}, c'v'\boldsymbol{k}') = [\varepsilon_c(\boldsymbol{k}) - \varepsilon_v(\boldsymbol{k})]\,\delta_{cc'}\delta_{vv'}\delta_{\boldsymbol{k}\boldsymbol{k}}$. Then the many-body effects can be added by improvement of the Hamiltonian in the next step according to the inclusion of quasiparticle shifts (8) and electron–hole interactions W (5) and $\bar{v}$ (6). In principle, the last step (including W and $\bar{v}$) can be done by diagonalizing the Hamiltonian matrix (4) [6, 8–10, 42].

However, we follow an earlier idea by Glutsch et al. [43] to calculate the polarizability from the time evolution of a vector $|\Psi(t)\rangle$ with N elements, which is defined as

$$\sum_{c',v',\boldsymbol{k}'} M^{j}_{c'v'}(\boldsymbol{k}')\, P(cv\boldsymbol{k}, c'v'\boldsymbol{k}'; \omega) = \frac{i}{\hbar}\int_0^\infty \mathrm{d}t\; \mathrm{e}^{i(\omega+i\gamma)t}\, \Psi_{cv\boldsymbol{k}}(t)\,. \tag{9}$$

The evolution of the elements of $|\Psi(t)\rangle$ are driven by the pair Hamiltonian (5)

$$\sum_{c',v',\boldsymbol{k}'} H(cv\boldsymbol{k}, c'v'\boldsymbol{k}')\, \Psi_{c'v'\boldsymbol{k}'}(t) = i\hbar\,\frac{\partial}{\partial t}\,\Psi_{cv\boldsymbol{k}}(t) \tag{10}$$

with their initial values

$$\Psi_{cv\boldsymbol{k}}(0) = M^{j}_{cv}(\boldsymbol{k})\,. \tag{11}$$

We solve the initial-value problem by the central difference method [14, 20]. The upper limit of the Fourier integral in (9) can be truncated due to the exponential $\exp(-\gamma t)$. The number of time steps, i.e., the matrix-vector multiplications, is nearly independent of the dimension of the system. The operation count for this method scales thus quadratically with the rank of the pair Hamiltonian, N. Details can be found in the paper [14].

3 Results and discussion

The total energies of the semiconductors with two atoms in the unit cell have been minimized. The resulting lattice constants are $a_0 = 3.538$ Å (C), 4.335 Å (SiC), 5.456 Å (Si), 5.413 Å (GaP), 5.615 Å (GaAs), 5.669 Å (InP), and 4.323 Å (AlN). For these theoretical lattice constants the Kohn–Sham (KS) eigenvalues have been computed. The resulting corresponding band structures are presented in the panels (a) of

© 2005 WILEY-VCH Verlag GmbH & Co. KGaA, Weinheim

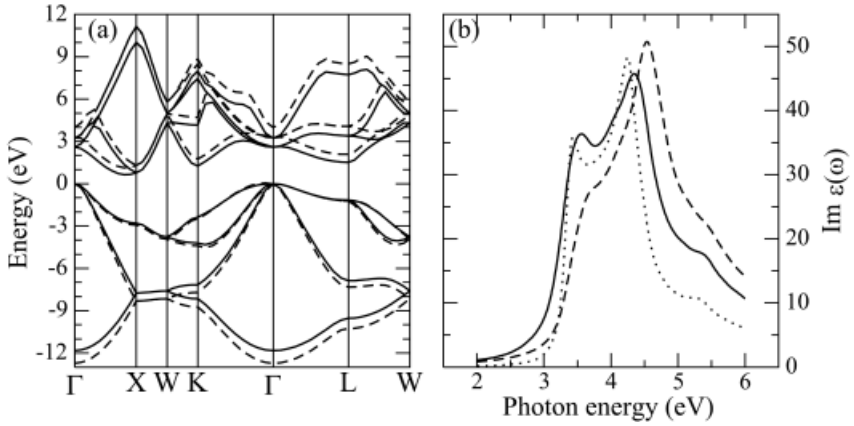

Fig. 5 Si: Experiment from [24].

Figs. 3–9. These energies as well as the Kohn–Sham wave functions have been used to calculate the high-frequency dielectric constant $\varepsilon_\infty = \varepsilon(0)$ within the independent-particle approximation, i.e., for a pair Hamiltonian (4) in the form $H(cv\boldsymbol{k}, c'v'\boldsymbol{k}') = [\varepsilon_c(\boldsymbol{k}) - \varepsilon_v(\boldsymbol{k})]\,\delta_{cc'}\delta_{vv'}\delta_{\boldsymbol{kk}}$. The results are close to experimental values $\varepsilon_\infty = 5.7$ (C), 7.1 (SiC), 11.3 (Si), 8.9 (GaP), 10.6 (GaAs), 9.6 (InP), and 4.4 (AlN).

This input determines the quasiparticle shifts. Together with the Kohn–Sham eigenvalues, they yield the QP band structures also shown in the panels (a) of Figs. 3–9. In a first approximation the QP corrections open all energy gaps and transition energies nearly by a rigid shift of the conduction bands with respect to the valence bands. This shift depends on the semiconductor. A typical value amounts to 0.8 eV as found for GaP. As a consequence all the optical spectra calculated within the independent-quasiparticle approximation (see panels (b) of Figs. 3–9) are blueshifted with respect to the independent-particle approximation (not shown) without dramatic changes of the lineshape. In the case of the common III–V semiconductors GaP, GaAs, and InP these spectra are very similar to the experimental ones (cf. Figs. 6–8). However, they are blueshifted, and the intensity of the high-energy E_2 peak is overestimated while that of the low-energy E_1 peak is underestimated. In the Si case (Fig. 5b) the E_1 peak appears only as a shoulder in the theoretical quasiparticle spectrum. For systems containing at least one constituent from the first row of the Periodic Table such as diamond, SiC, and AlN, the main peaks are too high in energy.

The inclusion of the excitonic and local-field effects has a remarkable influence on the theoretical spectra in Figs. 3–9 (panels (b)). For all materials a drastic redshift is observed with respect to the spectrum for independent quasiparticles. In general, this Coulomb shift is somewhat smaller than the average

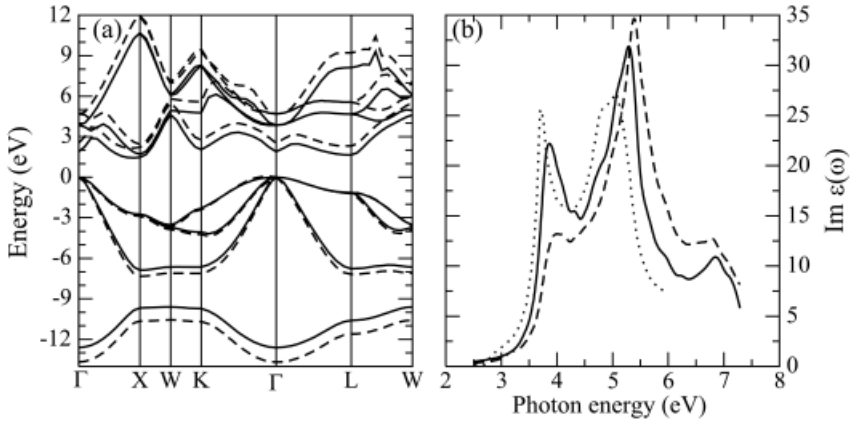

Fig. 6 GaP: Experiment from [46].

© 2005 WILEY-VCH Verlag GmbH & Co. KGaA, Weinheim

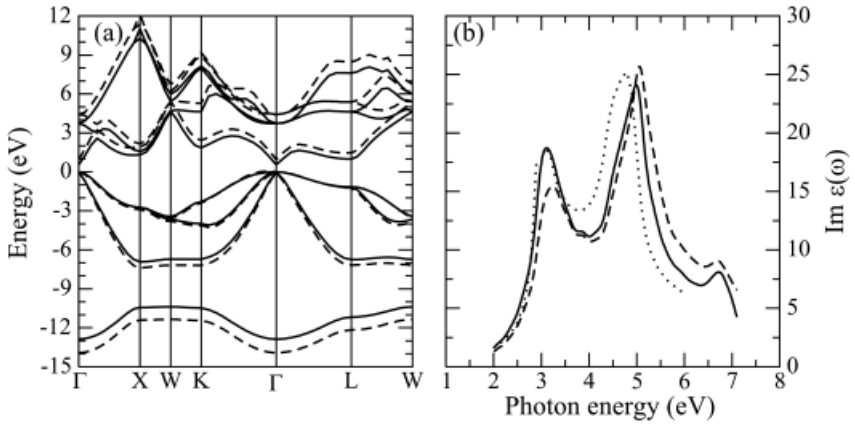

Fig. 7 GaAs: Experiment from [24].

quasiparticle blueshift. In the diamond case the ratio of the two effects is close to two, but it is strongly reduced for GaAs. All spectra indicate a drastic redistribution of oscillator strength/spectral strength from the high-energy region to the low-energy region. This effect is mainly a consequence of the Coulomb coupling of electron–hole pairs $cv\boldsymbol{k}$ and $c'v'\boldsymbol{k}'$ in the Hamiltonian (4). It modifies the scattering states of the electron–hole pair excitations. On the other hand, influences of bound exciton peaks are not visible in the spectra of Figs. 3–9. However, using much more refined $\boldsymbol{k}$-point meshes such excitonic peaks can be obtained below the onset of the absorption [8, 15].

The comparison of the theoretical spectra with quasiparticle effects and electron–hole interaction included with measured curves in panels (b) of Figs. 3–9 in general shows an excellent agreement with respect to the peak strengths and the peak positions for the semiconductors Si, GaP, GaAs, and InP with the pronounced E_1 and E_2 peaks in the imaginary part of the frequency-dependent dielectric function. The main failure of the theory is the overestimation of the peak positions by about 0.1 eV (III–V semiconductors) or 0.2 eV (Si). The agreement of the lineshape of the absorption spectra, in particular the peak positions, is also excellent in the case of cubic SiC. The comparison of the curves in Fig. 4b most drastically shows that experimental spectra can be only explained taking into account excitonic effects. The agreement in the case of diamond and cubic AlN is less satisfying. For diamond our approach overestimates the position of the central peak by about 0.7 eV, i.e., by about 5% of the peak energy. The discrepancy in the position of the main absorption peak between computation and experiment in Fig. 3b seems to be a general artefact of the theoretical description or the measurements for unknown reasons. In other excitonic calculations a similar discrepancy has been observed [9]. Only the scissors-operator ap-

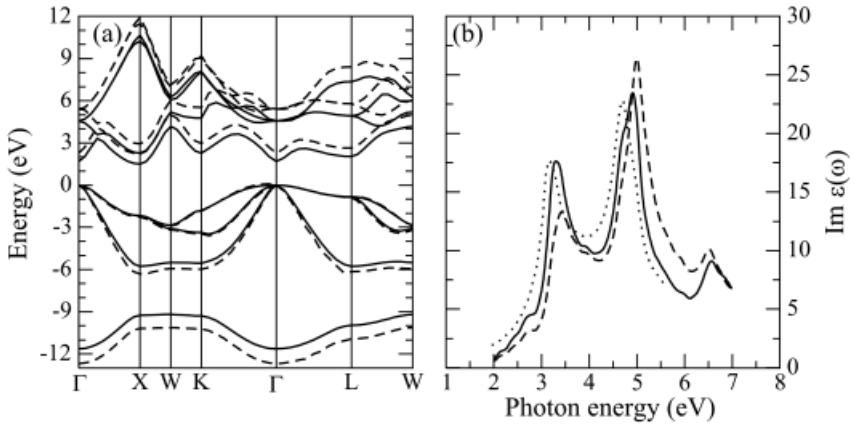

Fig. 8 InP: Experiment from [47].

© 2005 WILEY-VCH Verlag GmbH & Co. KGaA, Weinheim

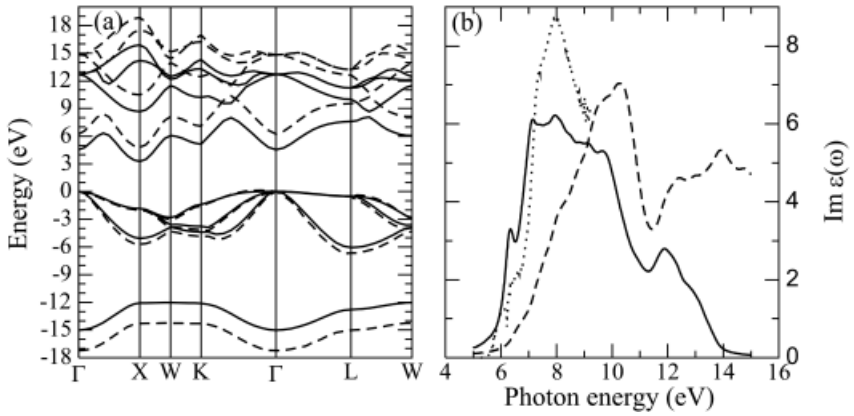

Fig. 9 Cubic AlN: Experiment from [48].

proach may give equal positions but give rise to an unphysical shift of the absorption edge [7]. However, in this case the absorption edge is redshifted by 0.5 eV, while our approach gives an absorption edge in agreement with the measurement [44]. In this volume of the journal there is another BSE calculation reported [49]. In the diamond case their agreement with the experiment is much better than here. One reason could be that the model GW approach tends to overestimate the QP shift for wide-gap materials by almost 0.2–0.3 eV. In the case of cubic AlN (Fig. 9b) further studies are needed. The role of the sample quality and perhaps screening effects by the polarizable lattice have to be clarified.

4 Summary

We have demonstrated the recent progress in the theoretical description of optical properties of crystalline materials using parameterfree computations under inclusion of the necessary many-body effects. The calculations are based on the density functional theory in a certain approximation for exchange and correlation. They yield the lattice constants (in general, the atomic positions) and the Kohn–Sham band structures which neglect the excitation aspect. After optical excitation of electron–hole pairs each excited particle interacts with the remaining electron system. This leads to a renormalization to a quasiparticle, quasielectron or quasi-hole. Its main effect is a shift of the Kohn–Sham eigenvalues towards quasiparticle energies and, hence, opens all gaps and transition energies. The quasielectrons and quasi-holes interact via two different mechanisms. There is a direct screened Coulomb attraction that yields an overall redshift of the absorption spectra with respect to curves for independent quasiparticles. Oscillator/spectral strength is redistributed from higher photon energies to lower ones. In addition, there also acts an electron–hole exchange that can be identified with the modelling of the local-field effects in the corresponding two-particle Hamiltonian. In any case, their inclusion allows to compute the macroscopic dielectric function instead of the microscopic one. They tend to reduce the redistribution of spectral strength from higher to lower photon energies but do less influence the peak positions. Local-field effects are larger for the wide-gap systems C and AlN in comparison to, for instance, Si.

Acknowledgements Grants of computer time from the Leibniz-Rechenzentrum München, the Höchstleistungsrechenzentrum Stuttgart, and the John von Neumann-Institut are gratefully acknowledged. This work has been supported by the EU through the Network of Excellence NANOQUANTA (Contract No. NMP4-CT-2004-500198) and the Deutsche Forschungsgemeinschaft (Project No.: Be 1346/18-1).

References

[1] G. Onida, L. Reining, and A. Rubio, Rev. Mod. Phys. **74**, 601 (2002).
[2] L. Hedin, Phys. Rev. A **139**, 796 (1965).
L. Hedin and S. Lundqvist, Solid State Phys. **23**, 1 (1969).

 © 2005 WILEY-VCH Verlag GmbH & Co. KGaA, Weinheim

[3] L. J. Sham and T. M. Rice, Phys. Rev. **144**, 708 (1966).
[4] W. Hanke and L. J. Sham, Phys. Rev. B **21**, 4656 (1980).
[5] G. Strinati, Riv. Nuovo Cimento **11**, 1 (1988).
[6] S. Albrecht, L. Reining, R. Del Sole, and G. Onida, Phys. Rev. Lett. **80**, 4510 (1998).
[7] L. X. Benedict, E. L. Shirley, and R. B. Bohn, Phys. Rev. Lett. **80**, 4514 (1998); Phys. Rev. B **57**, R9385 (1998).
[8] M. Rohlfing and S. G. Louie, Phys. Rev. Lett. **81**, 2312 (1998).
[9] B. Arnaud and M. Alouani, Phys. Rev. B **63**, 085208 (2001).
[10] P. Puschnig and C. Ambrosch-Draxl, Phys. Rev. B **66**, 165105 (2002).
[11] M. Rohlfing and S. G. Louie, Phys. Rev. Lett. **83**, 856 (1999).
[12] M. Rohlfing, M. Palummo, G. Onida, and R. Del Sole, Phys. Rev. Lett. **85**, 5440 (2000).
[13] P. H. Hahn, W. G. Schmidt, and F. Bechstedt, Phys. Rev. Lett. **88**, 016402 (2002).
[14] W. G. Schmidt, S. Glutsch, P. H. Hahn, and F. Bechstedt, Phys. Rev. B **67**, 085307 (2003).
[15] P. H. Hahn, W. G. Schmidt, K. Seino, M. Preuss, F. Bechstedt, and J. Bernholc, Phys. Rev. Lett. **94**, 037404 (2005).
[16] P. Hohenberg and W. Kohn, Phys. Rev. B **136**, 864 (1964).
[17] W. Kohn and L. J. Sham, Phys. Rev. A **140**, 1133 (1965).
[18] M. Fuchs and M. Scheffler, Comput. Phys. Commun. **119**, 67 (1999).
[19] E. L. Briggs, D. J. Sullivan, and J. Bernholc, Phys. Rev. B **54**, 14362 (1996).
[20] F. Bechstedt, W. G. Schmidt, and P. H. Hahn, phys. stat. sol. (a) **188**, 1383 (2001).
[21] G. Kresse and J. Furthmüller, Comput. Mater. Sci. **6**, 15 (1996); Phys. Rev. B **54**, 11169 (1996).
[22] G. Kresse and D. Joubert, Phys. Rev. B **59**, 1758 (1999).
[23] B. Adolph, J. Furthmüller, and F. Bechstedt, Phys. Rev. B **63**, 125108 (2001).
[24] D. E. Aspnes and A. A. Studna, Phys. Rev. B **27**, 985 (1983).
[25] F. Bechstedt, K. Tenelsen, B. Adolph, and R. Del Sole, Phys. Rev. Lett. **78**, 1528 (1997).
[26] G. D. Mahan, Many-Particle Physics (Plenum Press, New York, 1990).
[27] W. Hanke and L. J. Sham, Phys. Rev. B **12**, 4501 (1975).
[28] R. Del Sole and E. Fiorino, Phys. Rev. B **29**, 4631 (1984).
[29] S. Adler, Phys. Rev. **126**, 413 (1962).
[30] N. Wiser, Phys. Rev. **129**, 62 (1963).
[31] P. Hahn, Diploma thesis, Friedrich-Schiller-Universität, Jena (2001).
[32] M. S. Hybertsen and S. G. Louie, Phys. Rev. **34**, 5390 (1986).
[33] F. Bechstedt, Festkörperprobleme, Adv. Solid State Phys., Vol. 32 (Vieweg, Braunschweig, 1992), p. 161.
[34] O. Pulci, F. Bechstedt, G. Onida, R. Del Sole, and L. Reining, Phys. Rev. B **60**, 16758 (1999).
[35] M. S. Hybertsen and S. G. Louie, Phys. Rev. B **37**, 2733 (1988).
[36] F. Bechstedt, R. Del Sole, G. Cappellini, and L. Reining, Solid State Commun. **84**, 765 (1992).
[37] G. Cappellini, R. Del Sole, L. Reining, and F. Bechstedt, Phys. Rev. B **47**, 9892 (1993).
[38] W. G. Schmidt, J. L. Fattebert, J. Bernholc, and F. Bechstedt, Surf. Rev. Lett. **6**, 1159 (1999).
[39] H. J. Monkhorst and J. D. Pack, Phys. Rev. B **13**, 5188 (1976).
[40] F. Bechstedt, J. Furthmüller, P. H. Hahn, and F. Fuchs, J. Cryst. Growth (submitted).
[41] S. Albrecht, L. Reining, G. Onida, V. Olevano, and R. Del Sole, Phys. Rev. Lett. **83**, 3991 (1999).
[42] M. Rohlfing and S. G. Louie, Phys. Rev. B **62**, 4927 (2000).
[43] S. Glutsch, D. S. Chemla, and F. Bechstedt, Phys. Rev. B **54**, 11592 (1996).
[44] A. D. Papadopoulos and E. Anastassakis, Phys. Rev. B **43**, 5090 (1990).
[45] S. Logothetidis and J. Petalas, J. Appl. Phys. **80**, 1768 (1996).
[46] S. Zollner, M. Garriga, J. Kirchner, J. Humblícek, and M. Cardona, Phys. Rev. B **48**, 7915 (1993).
[47] P. Lautenschläger, M. Garriga, and M. Cardona, Phys. Rev. B **36**, 4813 (1987).
[48] R. Goldhahn, unpublished.
[49] O. Pulci et al., to appear in the same issue.

© 2005 WILEY-VCH Verlag GmbH & Co. KGaA, Weinheim